

Extended Reduced-order surrogate models for scalar-tensor gravity in the strong field and applications to binary pulsars and gravitational wave*

Minghao Guo, Junjie Zhao, and Lijing Shao[†]
Peking University, Beijing 100871, China

(MUSO Collaboration)

(Dated: December 9, 2020)

We investigate the scalar-tensor gravity of Damour and Esposito-Farèse (DEF) with spontaneous scalarization phenomena developed for neutron stars. We construct reduced-order surrogate model for the derived quantities and integrate the model into a python package pySTGROMX that speeds up calculations at two order-of-magnitude yet still keeps accuracy, compared with the previous method. The timing of binary pulsars allows us to place some of the tightest constraints on modified theories of gravity. We apply pySTGROMX to constrain the parameters of the DEF theory with well-timed binary pulsars.

I. INTRODUCTION

Albert Einstein's theory of general relativity (GR) has been tested in many cases, e.g., the Solar System, the timing of binary pulsars, and the gravitational-wave (GW) observation of coalescing binary black holes (BBHs) and binary neutron stars (BNSs).

Gravitational test has a long history.

In this paper, we design and develop a method for computing derived quantities in the scalar-tensor gravity of Damour and Esposito-Farèse (DEF) with spontaneous scalarization phenomena developed for neutron stars. We construct reduced-order surrogate model for the derived quantities and integrate the model into a python package pySTGROMX that speeds up calculations at two order-of-magnitude yet still keeps accuracy, compared with the previous method. The timing of binary pulsars allows us to place some of the tightest constraints on modified theories of gravity. We apply pySTGROMX to constrain the parameters of the DEF theory with well-timed binary pulsars.

II. SPONTANEOUS SCALARIZATION IN THE DEF THEORY

In this section, we study the DEF theory, which is defined by the following general action in *Einstein frame* [1, 2],

$$S = \frac{c^4}{16\pi G_\star} \int \frac{d^4x}{c} \sqrt{-g_\star} [R_\star - 2g_\star^{\mu\nu} \partial_\mu \varphi \partial_\nu \varphi - V(\varphi)] + S_m[\psi_m; A^2(\varphi)g_\star^{\mu\nu}]. \quad (1)$$

Here, G_\star denotes the bare gravitational constant, $g_\star \equiv \det g_\star^{\mu\nu}$ is the determinant of Einstein metric $g_\star^{\mu\nu}$, R_\star is the Ricci curvature scalar of $g_\star^{\mu\nu}$, and φ is a dynamical scalar field. In the last term of Eq. (1), ψ_m denotes matter fields collectively, and the conformal coupling factor $A(\varphi)$ describes how φ couples to ψ_m in Einstein frame. Varying the action (1) yields the field

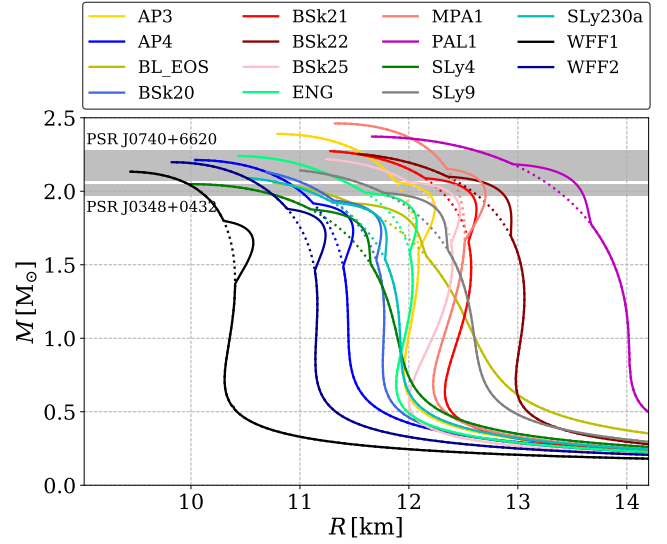


FIG. 1. Mass-radius relations of NSs for the EOSs that we adopt in this study. The mass-radius relations are derived from GR (dashed lines) and from a DEF theory with $\log_{10} |\alpha_0| = -5.0$ and $\beta_0 = -4.5$ (solid lines). The masses from PSRs J0740+6620 and J0348+0432 are overlaid in grey. The “bumps” show the deviation of the DEF theory from GR.

equations,

$$R_{\mu\nu}^\star = \partial_\mu \varphi \partial_\nu \varphi + \frac{8\pi G_\star}{c^4} (T_{\mu\nu}^\star - \frac{1}{2} T^\star g_{\mu\nu}^\star), \quad (2)$$

$$\square_{g^\star} \varphi = -\frac{4\pi G_\star}{c^4} \alpha(\varphi) T_\star, \quad (3)$$

where $T_\star^{\mu\nu} \equiv 2c(-g_\star)^{-1/2} \delta S_m / \delta g_\star^{\mu\nu}$ denotes the matter stress-energy tensor, and $T^\star \equiv g_\star^{\mu\nu} T_{\mu\nu}^\star$ is the trace. In Eq. (3), quantity $\alpha(\varphi)$ is defined as the logarithmic derivative of $A(\varphi)$,

$$\alpha(\varphi) \equiv \frac{\partial \ln A(\varphi)}{\partial \varphi}, \quad (4)$$

which indicates the coupling strength between the scalar field and matters.

In the DEF theory [2], $\ln A(\varphi)$ is designated as

$$\ln A(\varphi) = \frac{1}{2} \beta_0 \varphi^2. \quad (5)$$

* A footnote to the article title

[†] lshao@pku.edu.cn

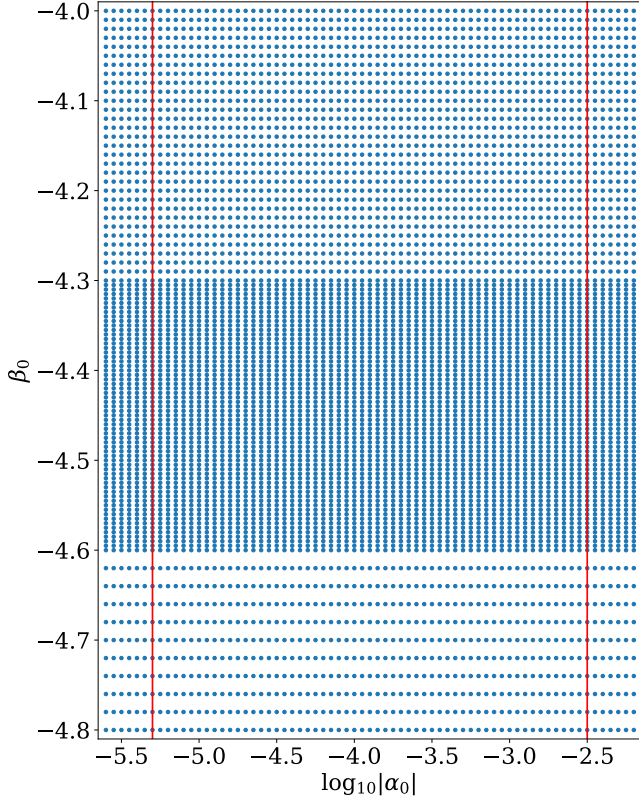


FIG. 2. An uneven grid in the parameter space ($\log_{10} |\alpha_0|, -\beta_0$) for calculating β_A and k_A and building ROMs. We generate a set of $69 \times 101 = 6969$ parameter pairs as the training data. The region between red lines corresponds to the data we use in later calculation.

Then $\alpha(\varphi) = \partial \ln A(\varphi) / \partial \varphi = \beta_0 \varphi$. We designate $\alpha_0 \equiv \beta_0 \varphi_0$, where φ_0 is the asymptotic scalar field value of φ at spatial infinity. Note that we have $\alpha_0 = \beta_0 = 0$ in GR. For NSs, nonperturbative scalarization phenomena develop when [1, 3]

$$\beta_0 \equiv \left. \frac{\partial^2 \ln A(\varphi)}{\partial \varphi^2} \right|_{\varphi=\varphi_0} \lesssim -4. \quad (6)$$

Generally, a more negative β_0 means more manifest spontaneous scalarization in the strong-field regime. In such case, the *effective scalar coupling* for a NS “A” with Arnowitt–Deser–Misner (ADM) mass m_A is

$$\alpha_A \equiv \left. \frac{\partial \ln m_A(\varphi)}{\partial \varphi} \right|_{\varphi=\varphi_0}, \quad (7)$$

which measures the coupling strength between the scalar field and the NS.

Now we consider a scalarized NS in a binary pulsar system. For a NS binary system with the pulsar labeled “A” and its companion labeled “B”, the quantities α_A and α_B contribute to the secular change of the orbital period decay \dot{P}_b [2]. Should

I write the exact formula here?

$$\dot{P}_b^{\text{dipole}} = -\frac{2\pi G_\star n_b}{c^3} g(e) \frac{m_A m_B}{m_A + m_B} (\alpha_A - \alpha_B)^2, \quad (8)$$

$$\dot{P}_b^{\text{quad}} = -\frac{192\pi G_\star^{5/3} n_b^{5/3}}{5c^5} f(e) \frac{m_A m_B}{(m_A + m_B)^{1/3}}, \quad (9)$$

where $n_b \equiv 2\pi/P_b$, and

$$g(e) \equiv (1 - e^2)^{-5/2} \left(1 + \frac{e^2}{2} \right), \quad (10)$$

$$f(e) \equiv (1 - e^2)^{-7/2} \left(1 + \frac{73}{24} e^2 + \frac{37}{94} e^4 \right). \quad (11)$$

Write the exact formula here. Correspondingly, we define

$$\beta_A \equiv \left. \frac{\partial \alpha_A}{\partial \varphi} \right|_{\varphi=\varphi_0}, \quad (12)$$

which is the strong-field analogue of the quantity β_0 . Then the theoretical prediction for the periastron advance rate is [2]

$$\begin{aligned} \dot{\omega}^{\text{th}}(m_A, m_B) &\equiv \frac{3n_b}{1 - e^2} \left(\frac{G_{AB}(m_A + m_B)n_b}{c^3} \right)^{2/3} \\ &\times \left[\frac{1 - \frac{1}{3}\alpha_A\alpha_B}{1 + \alpha_A\alpha_B} - \frac{X_A\beta_B\alpha_A^2 + X_B\beta_A\alpha_B^2}{6(1 + \alpha_A\alpha_B)^2} \right], \end{aligned} \quad (13)$$

where $G_{AB} \equiv G_\star(1 + \alpha_A\alpha_B)$, and $X_A \equiv m_A/(m_A + m_B) \equiv 1 - X_B$. Finally, consider a NS with inertia moment (in Einstein units) I_A . We denote

$$k_A \equiv \left. \frac{\partial \ln I_A}{\partial \varphi} \right|_{\varphi=\varphi_0} \quad (14)$$

as the “coupling factor” of inertia moment. The theoretical prediction of the Einstein delay parameter is [2],

$$\begin{aligned} \gamma \equiv \gamma^{\text{th}}(m_A, m_B) &= \frac{e}{n_b} \frac{X_B}{1 + \alpha_A\alpha_B} \left(\frac{G_{AB}(m_A + m_B)n_b}{c^3} \right)^{2/3} \\ &\times [X_B(1 + \alpha_A\alpha_B) + 1 + K_A^B], \end{aligned} \quad (15)$$

where $K_A^B \equiv -\alpha_B(m_B)k_A(m_A)$ describes the contribution from the variation of I_A under the influence of the companion B.

Maybe add a discussion about what kind of system (like binary NS) should be applied?

III. METHODOLOGY

We here turn our attention to the calculation of the quantities in strong field. For a specific nuclear EOS of NSs, given the center mass density ρ_c and the parameters of the theory (namely, α_0, β_0), we can obtain macroscopic quantities of a NS (e.g, R, m_A, α_A and I_A), by solving the modified TOV equations with the shooting method (see Ref. [4] for details). In Fig. 1 we show mass-radius relation of NSs in the DEF theory with $\log_{10} |\alpha_0| = -5.0$ and $\beta_0 = -4.5$ for the EOSs

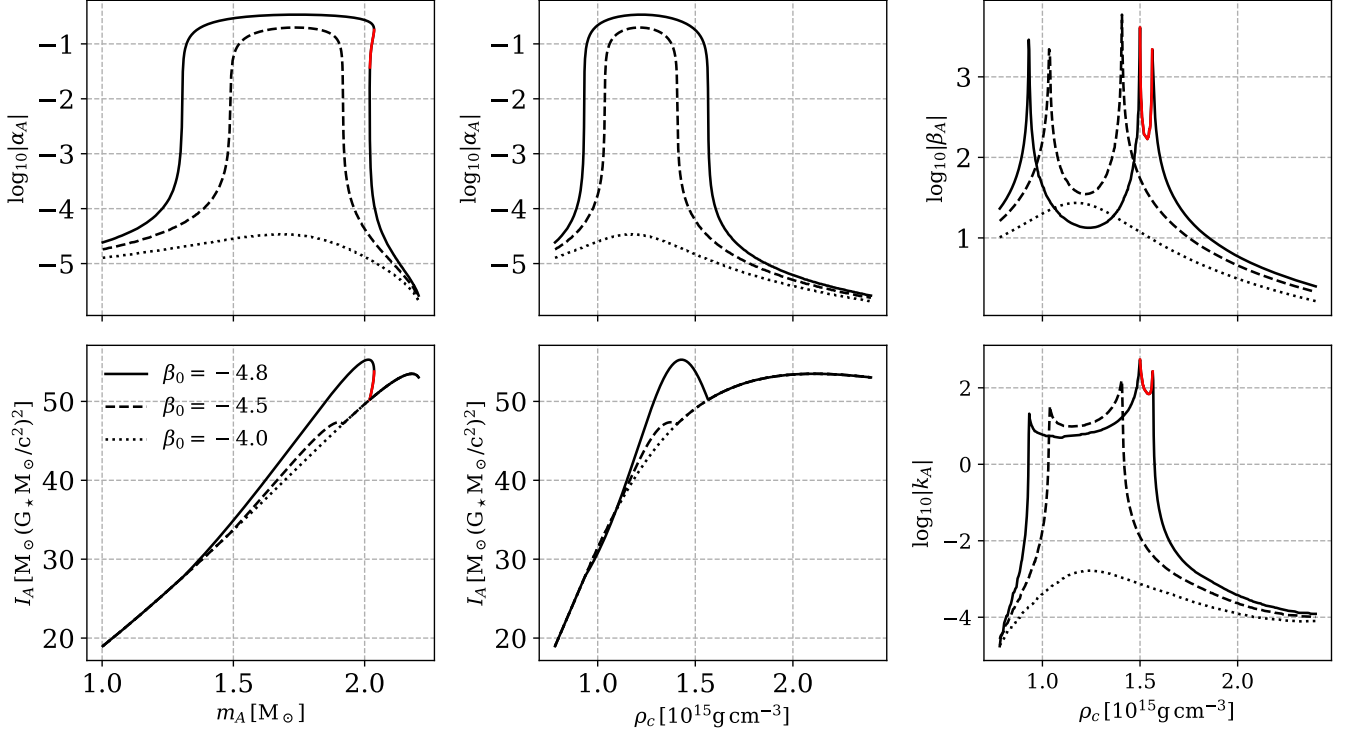


FIG. 3. Pathological phenomena occur when integrating the modified TOV equations for the EOS AP4. The calculation assumes the DEF parameters $\log_{10}|\alpha_0| = -5.3$ and $\beta_0 = -4.8$ (solid lines), -4.5 (dashed lines) and -4.0 (dotted lines). For $\log_{10}|\alpha_0| = -5.3$, the scalar field is weak for $\beta_0 = -4.0$, strong for $\beta_0 = -4.5$, and this causes the pathological phenomena for $\beta_0 = -4.8$. The red lines mark the pathological region. In this region, β_A and k_A are negative.

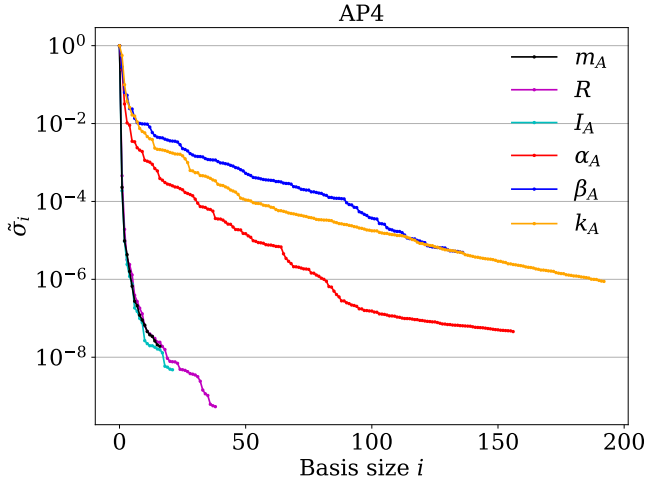


FIG. 4. Relative maximum projection error, $\tilde{\sigma}_i$, in building the ROMs for the EOS AP4. We set $\Sigma = 10^{-7}$ for m_A , R and I_A , $\Sigma = 10^{-5}$ for α_A , and $\Sigma = 10^{-4}$ for β_A and k_A .

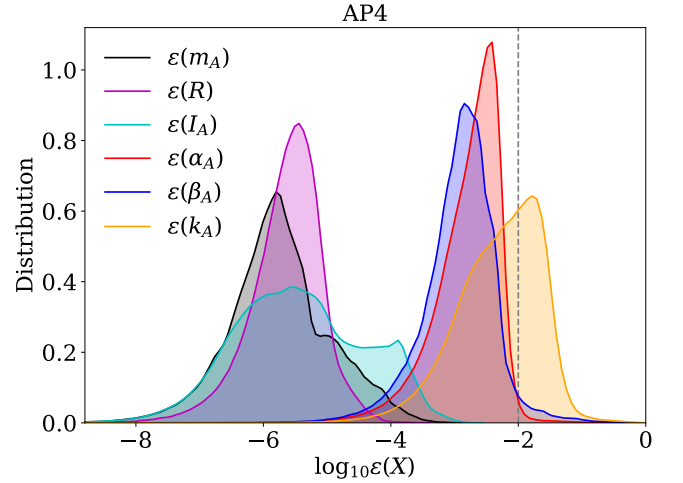


FIG. 5. Kernel density estimation (KDE) distribution of the relative error $\varepsilon(X)$, where $X \in \{m_A, R, I_A, \alpha_A, \beta_A, k_A\}$. The dashed line shows the relative tolerable error in the TOV integration ($\leq 1\%$).

we adopt in this study. It shows clearly that the spontaneous scalarization phenomena develop for NSs with certain masses, and larger radii are predicted in this range. However, to determine quantities β_A and k_A , we have to calculate the derivatives from Eqs. (12) and (14) for a fixed form of the conformal cou-

pling factor $A(\varphi)$ (i.e., with a fixed β_0) and a fixed baryonic mass \bar{m}_A . This requires the data with different φ_0 's (or equivalently, α_0 's). In order to do so, we calculate the derivatives on a grid. Should I show the PSR data in Fig.1? Also probably some data about the radius of NS.

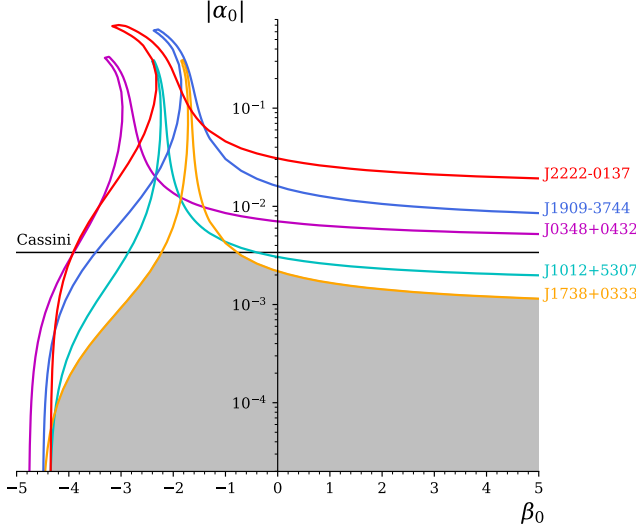


FIG. 6. Constraints on (α_0, β_0) from a variety of binary PSRs on DEF theory with the AP4 EOS. Cassini stands for the measurement of a Shapiro time-delay variation in the Solar system.

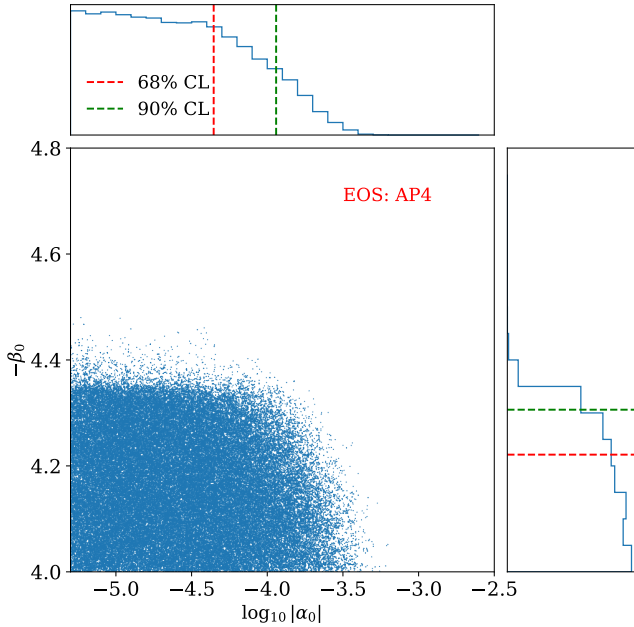


FIG. 7. The marginalized 2-dimensional distribution in the parameter space of $(\log_{10} |\alpha_0|, -\beta_0)$ in PSRs.

In practice, for each EOS, we choose the range of ρ_c so that $m_A \in (1 M_\odot, m_A^{\max})$ with the maximum NS mass m_A^{\max} being EOS-dependent. Then we generate an uneven grid of $[\log_{10} |\alpha_0|, \beta_0] \in [-5.6, -2.2] \times [-4.8, -4.0]$, as shown in Fig. 2. The number of nodes in grid is set to $N_{\alpha_0} \times N_{\beta_0} = 69 \times 101 = 6969$. We calculate β_A and k_A on each node with a reasonable differential step. Finally, we use the data of $\log_{10} |\alpha_0| \in [-5.3, -2.5]$ for further calculation to avoid the inaccuracy of derivatives at boundaries. The boundary value

$\alpha_0 \approx 10^{-2.5}$ is the upper limit given by the Cassini spacecraft [5], and $\beta_0 \lesssim -4.0$ corresponds to values where spontaneous scalarization happens in the DEF theory.

We have to point it out that in practice it is difficult to calculate k_A when the scalar field is weak. In this case, a change in I_A due to the weak field is comparable to the random noises during the integration in solving the modified TOV equations. The calculation of k_A is therefore not accurate. Here we propose a reasonable approximation that $k_A \sim \varphi_0^2$ when the spontaneous scalarization is not excited. Based on this assumption, we choose a large differential step and calculate $k_A = 2\varphi \partial \ln I_A / \partial \varphi^2$ to reduce the influence of numerical noises.

Due to the time-consuming computation of the TOV integration and the shooting method for large-scale calculations, such as the parameter estimation with the MCMC approach, we build ROMs for the quantities to improve the efficiency. In brief, to generate a ROM for a curve $h(t; \lambda)$ with parameters λ , one provides a training space of data $\mathbf{V} \equiv \{h(t; \lambda_i)\}$ on a given grid of parameters and select a certain number (denoted as m) of bases as a chosen space $\mathbf{RV} = \{e_i\}_{i=1}^m$ with the reduced basis (RB) method. In practice, given the starting RB ($i = 0$), one iteratively seeks for m orthonormal RBs by iterating the Gram-Schmidt orthogonalization algorithm with greedy selection to minimize the maximum projection error, [LS: references needed]

$$\sigma_i \equiv \max_{h \in \mathbf{V}} \|h(\cdot; \lambda) - \mathcal{P}_i h(\cdot; \lambda)\|^2, \quad (16)$$

where \mathcal{P} describes the projection of $h(t; \lambda)$ onto the span of the first i RBs. The process terminates when $\sigma_{m-1} \lesssim \Sigma$, a user-specified error bound. Then every curve in the training space is well approximated by

$$h(t; \lambda) \approx \sum_{i=1}^m c_i(\lambda) e_i(t) \approx \sum_{i=1}^m \langle h(\cdot; \lambda), e_i(\cdot) \rangle e_i(t), \quad (17)$$

where $c_i(\lambda)$ is the coefficient to be used for the ROM. Finally, one performs a fit to the parameter space, $\{\lambda_i\}$, and complete the construction of ROM. More details can be found in Ref. [4] where ROMs of α_A were built.

Extending the work by Zhao *et al.* [4], we build ROMs for six quantities, R , m_A , I_A , α_A , β_A and k_A , as functions of the central mass density ρ_c , with specialized parameters $\lambda = (\alpha_0, \beta_0)$.¹ We choose the implicit parameter ρ_c as an independent variable to avoid the the multivalued relations between m_A and R , as well as α_A and I_A [4]. We show this phenomena in Fig. 3. Due to the multivalued relations, β_A and k_A are negative when the α_A - m_A and I_A - m_A curve are bent backwards.

In balancing the computation cost and the accuracy of ROMs, we set the error bound $\Sigma = 10^{-7}$ for m_A , R and I_A ,

¹ In practice, we use $\ln |I_A|$, $\ln |\alpha_A|$, $\ln |\beta_A|$, and $\ln |k_0 + k_A|$ —instead of β_A and k_A —for a better numerical performance, where k_0 is an EOS-dependent constant to avoid negative values of k_A in the weak field. Generally we have $k_0 \lesssim 0.1$.

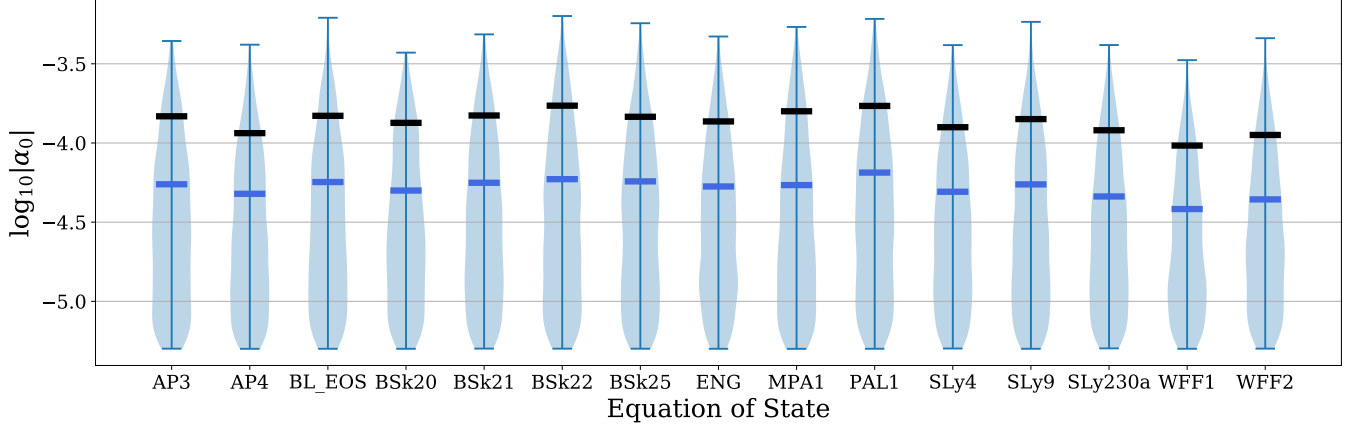


FIG. 8. The marginalized distribution in the parameter space of $(\log_{10} |\alpha_0|)$ in PSRs for 15 EOSs in our studies. The 90% and 68% CL upper bounds are shown by the black and blue bars. Notice that the limit on $|\alpha_0|$ is affected by our priors (see text).

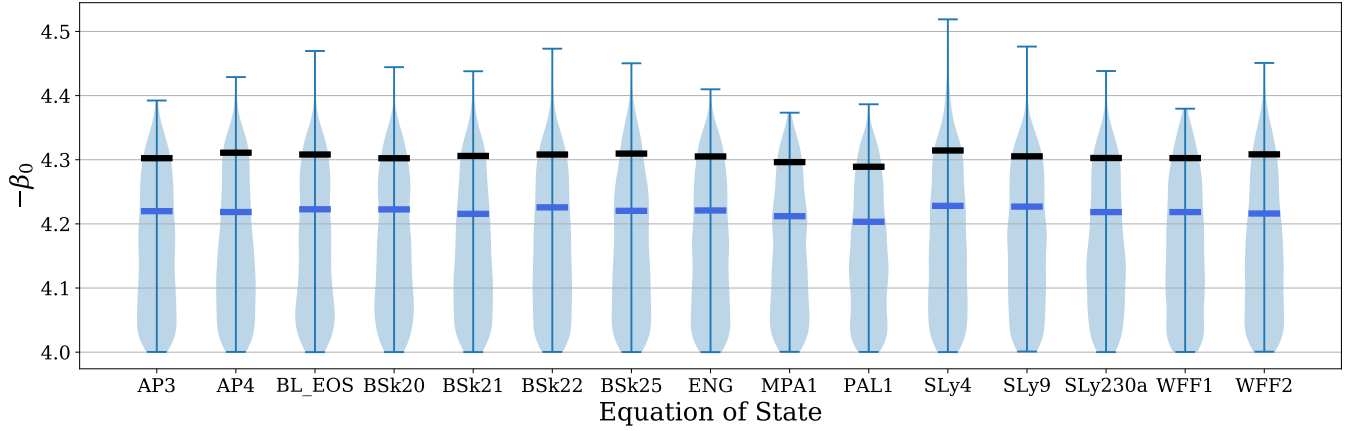


FIG. 9. Same as Fig. 8, but for the parameter $-\beta_0$.

$\Sigma = 10^{-5}$ for α_A , and $\Sigma = 10^{-4}$ for β_A and k_A . The relative projection error $\tilde{\sigma}_i \equiv \sigma_i/\sigma_0$ as a function of the basis size is shown in Fig. 4. To achieve the desired projection error, the basis size is ~ 20 -40 for m_A , R and I_A , but ~ 150 -200 for α_A , β_A and k_A . This is due to the fact that there are more features in the latter set of parameters. Considering the error involved in the shooting method and the calculation of derivatives, which is $\sim 1\%$, the precision loss in ROM building is negligible. But, $\varepsilon(k_A)$ is much larger than 0.01, maybe we should point it out. About $\varepsilon(k_A)$, since we build ROM for $\ln|k_A + k_0|$, is it reasonable to build assess the accuracy using Eq. 18?

To assess the accuracy of the ROMs, we define

$$\varepsilon(X) = \left| \frac{X_{\text{ROM}} - X_{\text{mTOV}}}{X_{\text{ROM}} + X_{\text{mTOV}}} \right|, \quad (18)$$

where $X \in \{m_A, R, I_A, \alpha_A, \beta_A, k_A\}$, to indicate the fractional accuracy of the ROMs. In Eq. (18), we denote X_{ROM} as the prediction of ROM, and X_{mTOV} as the value from the shooting algorithm and derivatives on the grid. Explain why choosing grid here. To calculate the derivatives, instead of randomly generating parameters, we choose another grid as the

test space which is shifted from the training space for α_0, β_0 and ρ_c , and calculate the quantities in the same way. Note that in this method we include all errors for our ROMs, including the interpolating errors. We should explain why we test the parameters shifted in training space instead of random space. The test space has sparser distribution of β_0 . The distributions of $\varepsilon(X)$ are shown in Fig. 5. The relative errors of m_A , R and I_A are $\lesssim 10^{-5}$. On the contrary, relative errors of α_A , β_A and k_A is mostly smaller than 1%. Although this error is larger than those of R and m_A , in most cases, the error is still small enough to be neglected compared with the error from the shooting method and the calculation of derivatives. About the error: For k_A , due to the additional error from the method in calculating the derivatives, a small fraction of prediction have the error in the range $\sim 1 - 10\%$.

IV. CONSTRAINTS FROM BINARY PULSARS

In this section, we apply our ROMs to various scenarios, and discuss the improvement in deriving NS properties. We

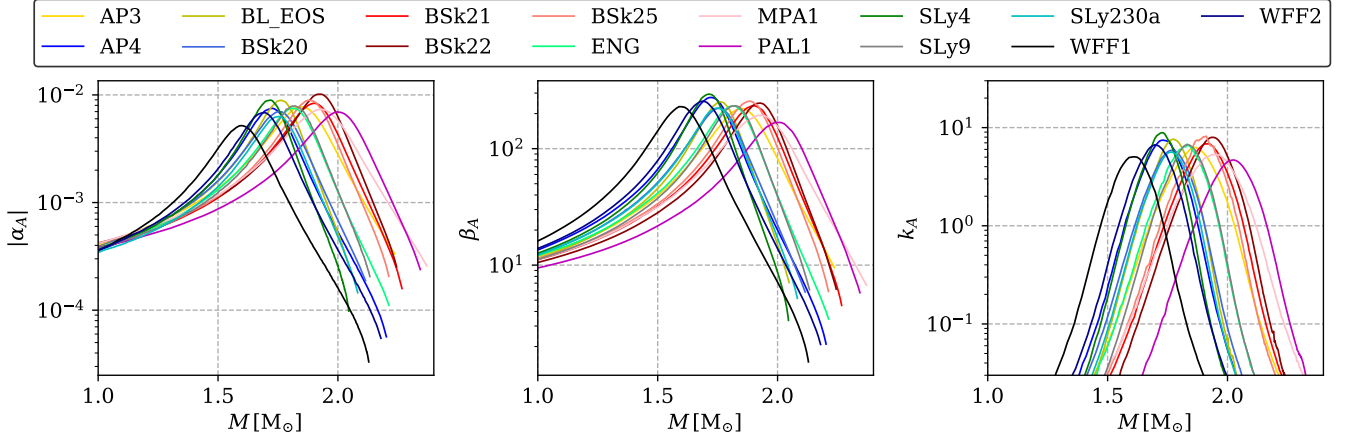


FIG. 10. The 90% CL upper bounds on the NS effective scalar coupling, α_A , β_A and k_A .

TABLE I. Binary parameters of the five NS-WD systems that we use to constrain the DEF theory.

Name	J0348+0432	J1012+5307	J1738+0333	J1909-3744	J2222-0137
Orbital period, P_b (d)	0.102424062722(7)	0.60467271355(3)	0.3547907398724(13)	1.533449474305(5)	2.44576454(18)
Eccentricity, e	0.0000026(9)	0.0000012(3)	0.00000034(11)	0.000000115(7)	0.00038096(4)
Observed \dot{P}_b , \dot{P}_b^{obs} (fs s $^{-1}$)	-273(45)	50(14)	-17.0(31)	-510.87(13)	200(90)
Intrinsic \dot{P}_b , \dot{P}_b^{int} (fs s $^{-1}$)	-274(45)	-5(9)	-27.72(64)	-4.4(79)	-60(90)
Periastron advance, $\dot{\omega}$ (deg yr $^{-1}$)	—	—	—	—	0.1001(35)
Einstein delay γ (ms)	—	—	—	—	—
Pulsar mass, m_p (M_\odot)	2.01(4)	—	—	1.492(14)	1.76(6)
Companion mass, m_c (M_\odot)	0.1715 $^{+0.0045}_{-0.0030}$	0.174(7)	0.1817 $^{+0.0073}_{-0.0054}$	0.209(1)	1.293(25)
Mass ratio, $q \equiv m_p/m_c$	11.70(13)	10.5(5)	8.1(2)	—	—

combine observational results from multiple pulsar systems employing Markov chain Monte Carlo (MCMC) simulations. The efficiency is much higher than previous calculation.

To be finished...

A. Set up

In Table I, we show five well-timing NS-WD binary pulsars, whose mass is measured independently, in testing spontaneous scalarization: PSRs J0348+0432 [6], J1012+5307 [7–10], J1738+0333 [11], J1909-3744 [12], J2222-0137 [13].

Thus we get a satisfying results. The WD companion is a weakly self-gravitating object, leading to a tiny effective scalar coupling $\alpha_c \approx \alpha_0$. This leads to a large dipole contribution, $\propto (\alpha_A - \alpha_0)^2$, to the orbital period decay.

In Table II, we show three double NSs, PSRs B1913+16 [14], J0737-3039A [15], J1757-1854 [16]. Need some detailed discussion about the detailed choice and parameters here. The pulsar parameters and orbit parameters are measured by the TOA of pulses, including Keplerian and post-Keplerian parameters. Some parameters, such as the time derivative of the orbital period, \dot{P}_b , Periastron advance $\dot{\omega}$, Einstein delay γ are functions of the masses, and thus can be utilized to constrain the free parameters of DEF theory, α_0 and β_0 .

In this study, we adopt 16 EOSs, AP3, AP4, BL_EOS,

BSk20, BSk21, BSk22, BSk25, ENG, H4, MPA1, PAL1, SLy4, SLy9, SLy230a, WFF1, WFF2, as shown in Fig. 1. They are all consistent with the observe $2M_\odot$ maximum mass limit of NS. In addition, we adopt more EOS with radius around ~ 11 -13 km, owing to recent discovery about radius of NS.

It is worth noting that a completely new era for testing highly dynamical strong field with NSs has began with GW170817, thus these parameters can be used in the future detection.

B. 1- σ constraints

First, we estimate the constraint on the DEF parameters α_0 and β_0 by saturating the bounds on individual post-Keplerian parameters. However, we need to assume a particular EOS for these constraints. From the measurements of \dot{P}_b , we constrain α_A and α_B by evaluating Eqs. 8 and 9. Then we further constrain $(|\alpha_0|, \beta_0)$ in region $[-5.0, 0] \times [-5.0, 5.0]$. By determining if the predicted value \dot{P}_b^{th} lie within the $1 - \sigma$ range of \dot{P}_b , i.e., $\dot{P}_b \pm \delta\dot{P}_b$, we can obtain the limits on the parameter space.

In 6, we show the constraints on α_0 and β_0 for binary pulsars, assuming a EOS of AP4. Note that these constraints are dependent on the specific EOS. The results are similar to

TABLE II. Binary parameters of the three NS-NS systems that we use to constrain the DEF theory.

Name	B1913+16	J0737-3039A	J1757-1854
Orbital period, P_b (d)	0.322997448918(3)	0.10225156248(5)	0.18353783587(5)
Eccentricity, e	0.6171340(4)	0.0877775(9)	0.6058142(10)
Observed \dot{P}_b , \dot{P}_b^{obs} (fs s ⁻¹)	-2423(1)	-1252(17)	-5300(200)
Intrinsic \dot{P}_b , \dot{P}_b^{int} (fs s ⁻¹)	-2398(4)	-1252(17)	-5300(240)
Periastron advance, $\dot{\omega}$ (deg yr ⁻¹)	4.226585(4)	16.89947(68)	10.3651(2)
Einstein delay γ (ms)	4.307(4)	0.3856(26)	3.587(12)
Pulsar mass, m_p (M _⊙)	1.438(1)	1.3381(7)	1.3384(9)
Companion mass, m_c (M _⊙)	1.390(1)	1.2489(7)	1.3946(9)
Mass ratio, $q \equiv m_p/m_c$	—	—	—

previous results in [11, 17]. This diagrammatically illustrates the constraints from the timing parameters on the DEF theory. However, to determine the constraint in the strong field ($\beta_0 < -4.0$) in more details, we need more accurate method.

C. Bayesian inference

We here explore constraints on the DEF theory with the well-timed binary pulsars through MCMC simulations.

In the Bayesian inference, given hypothesis \mathcal{H} , data \mathcal{D} , and priors, the posterior distribution of (α_0, β_0) can be inferred by

$$P(\alpha_0, \beta_0 | \mathcal{D}, \mathcal{H}, \mathcal{I}) = \int \frac{P(\mathcal{D} | \alpha_0, \beta_0, \Xi, \mathcal{H}, \mathcal{I}) P(\alpha_0, \beta_0 | \Xi | \mathcal{H}, \mathcal{I})}{P(\mathcal{D} | \mathcal{H}, \mathcal{I})} d\Xi,$$

(19)

where \mathcal{I} is all the extra relevant information.

For our studies, we carefully choose the priors of (α_0, β_0) so as to cover the the region where the spontaneous scalarization develops. We assume a uniform distribution of $(\log_{10} |\alpha_0|, \beta_0)$ in the region of our ROMs. Then the parameters can be constrained by evaluating the log-likelihood function.

For binary pulsars, the general log-likelihood function is

$$\ln \mathcal{L}_{\text{PSR}} = -\frac{1}{2} \sum_{i=1}^{N_{\text{PSR}}} \left[\left(\frac{\dot{P}_b^{\text{th}} - \dot{P}_b^{\text{int}}}{\sigma_{\dot{P}_b^{\text{int}}}} \right)^2 + \left(\frac{\dot{\omega} - \dot{\omega}^{\text{obs}}}{\sigma_{\dot{\omega}}} \right)^2 + \left(\frac{\gamma - \gamma^{\text{obs}}}{\sigma_{\gamma^{\text{obs}}}} \right)^2 + \left(\frac{m_p - m_p^{\text{obs}}}{\sigma_{m_p^{\text{obs}}}} \right)^2 + \left(\frac{m_c - m_c^{\text{obs}}}{\sigma_{m_c^{\text{obs}}}} \right)^2 \right] \quad (20)$$

for N_{PSR} bianry pulsar systems. In a short summary, the likelihood function include all contributions. However, not each pulsar's measurement of \dot{P}_b , $\dot{\omega}$, γ , m_p and m_c are independent. Thus, for some pulsars, the contribution are not counted.

For the full calculation, we note that, for some parameters, like the orbital period P_b and the orbital eccentricity, e , we adopt their central value since they are determined very well.

For the MCMC runs, we use a uniform prior on the region of our ROMs, i.e., $\alpha_0 \in [-5.6, -2.2]$, $\beta_0 \in [-4.8, -4.0]$. During the whole process, we restrict the parameters in this region of interest. Now, we employ MCMC technique to get the posteriors from the priors on (α_0, β_0) and the log-likelihood function. The initial values of central matter densities, ρ_c , are needed in the Jordan frame. They are fed to our ROMs to derive the NS properties. Initially they will be sampled around their GR values, but they are allowed to explore a sufficiently large range in the MCMC process. We use 24 walkers and 100000 steps for each MCMC simulation.

We perform Gelman-Rubin test for convergence and our

D. Constraints from binary pulsars

In Fig. 7, we show the marginalized 2-d posterior distribution in the parameter space of $(\log_{10} |\alpha_0|, -\beta_0)$. The results are similar to previous constraints.

In addition to the five NS-WD bianry pulsars, that have been investigated very well in [4], we combine three extra double NS system, which utilize the information from $\dot{\omega}$ and γ .

For each EOS, we perform MCMC runs with different combination of observations. The scenarios are shown in Table I.

In Fig. 8 and Fig. 9, we show the distribution of $\log_{10} |\alpha_0|$ and $-\beta_0$ for all the 15 EOSs, and their 68% and 90% CL upper bounds. The constraints on α_0 is highly influenced by the priors. But the *relative* strength of these tests does not change. A

more stiff EOS would generally lead to more tight constraints.

V. CONCLUSION

In Fig. 10, the 90% CL upper bounds on the NS shows that the “scalarization window” [17] is still open, though slightly limited. However, the peak of β_A shown in Fig. 3 is strongly excluded. Therefore a large deviation from GR is not expected.

In this paper, we investigated the scalar-tensor gravity theory proposed by Damour and Esposito-Farèse (DEF) that predicts large deviations from General Relativity for neutron stars through spontaneous scalarization phenomena. we constructed reduced-order surrogate model for the derived quantities $m_A, R, I_A, \alpha_A, \beta_A, k_A$ in this theory, coded in a python package pySTGROMX that speeds up calculations at two orders of magnitude yet still keeps accuracy, compared with the previous algorithms. The code is made public for the community use. As an application, we utilized pySTGROMX to explore constraints on the DEF theory with latest well-timed binary pulsars and gravitational waves through MCMC simulations. We show that the “scalarization window” is still open.

-
- [1] T. Damour and G. Esposito-Farèse, *Phys. Rev. Lett.* **70**, 2220 (1993).
 - [2] T. Damour and G. Esposito-Farèse, *Phys. Rev. D* **54**, 1474 (1996).
 - [3] E. Barausse, C. Palenzuela, M. Ponce, and L. Lehner, *Phys. Rev. D* **87**, 081506 (2013).
 - [4] J. Zhao, L. Shao, Z. Cao, and B.-Q. Ma, *Phys. Rev. D* **100**, 064034 (2019).
 - [5] B. Bertotti, L. Iess, and P. Tortora, *Nature* **425**, 374 (2003).
 - [6] J. Antoniadis, P. C. C. Freire, N. Wex, T. M. Tauris, R. S. Lynch, M. H. van Kerkwijk, M. Kramer, C. Bassa, V. S. Dhillon, T. Driebe, J. W. T. Hessels, V. M. Kaspi, V. I. Kondratiev, N. Langer, T. R. Marsh, M. A. McLaughlin, T. T. Pennucci, S. M. Ransom, I. H. Stairs, J. van Leeuwen, J. P. W. Verbiest, and D. G. Whelan, *Science* **340**, 448 (2013), [arXiv:1304.6875 \[astro-ph.HE\]](#).
 - [7] K. Lazaridis, N. Wex, A. Jessner, M. Kramer, B. W. Stappers, G. H. Janssen, G. Desvignes, M. B. Purver, I. Cognard, G. Theureau, A. G. Lyne, C. A. Jordan, and J. A. Zensus, *Mon. Not. R. Astron. Soc.* **400**, 805 (2009), [arXiv:0908.0285 \[astro-ph.GA\]](#).
 - [8] G. Desvignes, R. N. Caballero, L. Lentati, J. P. W. Verbiest, D. J. Champion, B. W. Stappers, G. H. Janssen, P. Lazarus, S. Osłowski, S. Babak, C. G. Bassa, P. Brem, M. Burgay, I. Cognard, J. R. Gair, E. Graikou, L. Guillemot, J. W. T. Hessels, A. Jessner, C. Jordan, R. Karuppusamy, M. Kramer, A. Lassus, K. Lazaridis, K. J. Lee, K. Liu, A. G. Lyne, J. McKee, C. M. F. Mingarelli, D. Perrodin, A. Petiteau, A. Possenti, M. B. Purver, P. A. Rosado, S. Sanidas, A. Sesana, G. Shaifullah, R. Smits, S. R. Taylor, G. Theureau, C. Tiburzi, R. van Haasteren, and A. Vecchio, *Mon. Not. R. Astron. Soc.* **458**, 3341 (2016), [arXiv:1602.08511 \[astro-ph.HE\]](#).
 - [9] J. Antoniadis, T. M. Tauris, F. Özel, E. Barr, D. J. Champion, and P. C. C. Freire, *arXiv e-prints*, [arXiv:1605.01665 \(2016\)](#), [arXiv:1605.01665 \[astro-ph.HE\]](#).
 - [10] D. Mata Sánchez, A. G. Istrate, M. H. van Kerkwijk, R. P. Breton, and D. L. Kaplan, *Mon. Not. R. Astron. Soc.* **494**, 4031 (2020), [arXiv:2004.02901 \[astro-ph.HE\]](#).
 - [11] P. C. C. Freire, N. Wex, G. Esposito-Farèse, J. P. W. Verbiest, M. Bailes, B. A. Jacoby, M. Kramer, I. H. Stairs, J. Antoniadis, and G. H. Janssen, *Mon. Not. R. Astron. Soc.* **423**, 3328 (2012), [arXiv:1205.1450 \[astro-ph.GA\]](#).
 - [12] K. Liu, L. Guillemot, A. G. Istrate, L. Shao, T. M. Tauris, N. Wex, J. Antoniadis, A. Chalumeau, I. Cognard, G. Desvignes, P. C. C. Freire, M. S. Kehl, and G. Theureau, *Mon. Not. R. Astron. Soc.* **499**, 2276 (2020), [arXiv:2009.12544 \[astro-ph.HE\]](#).
 - [13] I. Cognard, P. C. C. Freire, L. Guillemot, G. Theureau, T. M. Tauris, N. Wex, E. Graikou, M. Kramer, B. Stappers, A. G. Lyne, C. Bassa, G. Desvignes, and P. Lazarus, *Astrophys. J.* **844**, 128 (2017), [arXiv:1706.08060 \[astro-ph.HE\]](#).
 - [14] J. M. Weisberg and Y. Huang, *Astrophys. J.* **829**, 55 (2016), [arXiv:1606.02744 \[astro-ph.HE\]](#).
 - [15] M. Kramer, I. H. Stairs, R. N. Manchester, M. A. McLaughlin, A. G. Lyne, R. D. Ferdman, M. Burgay, D. R. Lorimer, A. Possenti, N. D’Amico, J. M. Sarkissian, G. B. Hobbs, J. E. Reynolds, P. C. C. Freire, and F. Camilo, *Science* **314**, 97 (2006), [arXiv:astro-ph/0609417 \[astro-ph\]](#).
 - [16] A. D. Cameron, D. J. Champion, M. Kramer, M. Bailes, E. D. Barr, C. G. Bassa, S. Bhandari, N. D. R. Bhat, M. Burgay, S. Burke-Spolaor, R. P. Eatough, C. M. L. Flynn, P. C. C. Freire, A. Jameson, S. Johnston, R. Karuppusamy, M. J. Keith, L. Levin, D. R. Lorimer, A. G. Lyne, M. A. McLaughlin, C. Ng, E. Petroff, A. Possenti, A. Ridolfi, B. W. Stappers, W. van Straten, T. M. Tauris, C. Tiburzi, and N. Wex, *Mon. Not. R. Astron. Soc.* **475**, L57 (2018), [arXiv:1711.07697 \[astro-ph.HE\]](#).
 - [17] L. Shao, N. Sennett, A. Buonanno, M. Kramer, and N. Wex, *Physical Review X* **7**, 041025 (2017), [arXiv:1704.07561 \[gr-qc\]](#).